



HAL
open science

Selective elimination of phenol from hydrocarbons by zeolites and silica-based adsorbents-Impact of the textural and acidic properties

Ibrahim Khalil, Karine Thomas, Hicham Jabraoui, Philippe Bazin, Françoise Maugé

► **To cite this version:**

Ibrahim Khalil, Karine Thomas, Hicham Jabraoui, Philippe Bazin, Françoise Maugé. Selective elimination of phenol from hydrocarbons by zeolites and silica-based adsorbents-Impact of the textural and acidic properties. *Journal of Hazardous Materials*, 2020, 384, pp.121397. 10.1016/j.jhazmat.2019.121397 . hal-02345827

HAL Id: hal-02345827

<https://hal.science/hal-02345827>

Submitted on 17 Dec 2020

HAL is a multi-disciplinary open access archive for the deposit and dissemination of scientific research documents, whether they are published or not. The documents may come from teaching and research institutions in France or abroad, or from public or private research centers.

L'archive ouverte pluridisciplinaire **HAL**, est destinée au dépôt et à la diffusion de documents scientifiques de niveau recherche, publiés ou non, émanant des établissements d'enseignement et de recherche français ou étrangers, des laboratoires publics ou privés.

1 **Selective elimination of phenol from hydrocarbons by zeolites and**
2 **silica-based adsorbents – Impact of the textural and acidic properties**

3 Ibrahim Khalil¹, Karine Thomas^{1*}, Hicham Jabraoui², Philippe Bazin¹, Françoise Mauge¹

4 ¹ Laboratoire Catalyse et Spectrochimie, ENSICAEN, Université de Caen Normandie, CNRS, 6, bd du
5 Maréchal Juin, 14050 Caen, France

6 ² Laboratoire Physique et Chimie Théoriques (LPCT) UMR 7019 CNRS, Université de Lorraine, F-
7 54000 Nancy, France

8 * corresponding author: karine.thomas@ensicaen.fr

9

10 Keywords: Phenol adsorption; Toluene adsorption; Selectivity; Zeolite acidity; Breakthrough curves;

11 Highlights:

- 12 - Phenol condensed in Y zeolite supercages but adsorbed on external silanol groups
- 13 - HY selectively adsorbed phenol in presence of toluene and linear hydrocarbon
- 14 - Easy regeneration requires low amount of acidic sites

15

16 **ABSTRACT**

17 This paper investigates the parameters that influence the selective adsorption of phenol, toxic
18 molecule, from a semi-model biofuel mixture containing alkanes and different proportions of aromatic
19 compounds. The adsorption capacity, selectivity and regeneration ability of different adsorbents, i.e.
20 zeolites, silica-based solids, alumina and activated carbon, were related to their textural properties and
21 to the nature, strength or location of their acidic sites. This work demonstrates that phenol differently
22 adsorbs in the micropores and mesopores. In the micropores of faujasites, phenol is condensed into the
23 supercages. Otherwise, in the mesopores of the zeolite, phenol interacts with the silanol groups. On
24 purely siliceous adsorbents, a ratio of one phenol adsorbed on one silanol group could be established.
25 As for selectivity, the strong acidic sites of the faujasites are necessary to favor phenol adsorption
26 compared to toluene one. By contrast, the amount of strong Brønsted and Lewis acid sites limits
27 regeneration. Hence, a compromise has to be found and the best performances were obtained using a
28 slightly dealuminated zeolitic adsorbent presenting both micro and mesopores.

29

30 **1. INTRODUCTION**

31 Global energy demand is expected to grow by around the third between 2018 and 2040 [1], resulting
32 an increase in the fossil fuel consumption known as the most common source of energy on our planet
33 [2]. However, the serious environmental changes (global warming), caused by the CO₂ emissions
34 produced after burning the fossil fuels in vehicles, restrict their excessive use in the next years [3–5].
35 For such a purpose, governments around the world has raised concerns and increased the focus on the
36 research for the development of environmentally friendly renewable sources of fuel and energy [6].

37 New generations of transportation biofuels have recently been introduced, involving a partial or
38 complete replacement of fossil fuels by renewable resources as those derived from biomass [7].
39 Biofuels of first generation are produced from food and agriculture [3]. They are currently used in
40 many countries as pure fuel source (e.g. bioethanol) or in mixtures with fossil fuels (e.g. biodiesel) [8].
41 They contribute in the reduction of green-house-gas emissions but they create a negative impact on
42 food security [9]. Nowadays, a significant effort is deployed on processing second generation biofuel
43 production i.e. that is issued from non-edible biomass [3], as lignocellulosic biomass from wood and
44 agricultural wastes [10]. Oils obtained from the pyrolysis of this biomass present similar
45 physicochemical and rheological properties to crude oils [4]. However, their high viscosity,
46 corrosiveness and low energetic power related to their high oxygen content (20 - 55 wt.%) limit their
47 uses [2,11]. Therefore to obtain bio-oils compatible with the crude oil feedstock, oxygen should be
48 removed [12,13]. In this way, pyrolytic bio-oils can be upgraded by a first hydrodeoxygenation (HDO)
49 step. The upgraded bio-oils are further co-proceeded with a vacuum gas oil (VGO) in a fluid cracking
50 catalytic (FCC) unit [14]. Due to the hydrogen transfer occurring during FCC process, the cracking
51 products contain a lower amount of oxygen (0.5 wt.% to 7 wt.%), mainly composed of substituted
52 phenol type molecules [7,8]. However, phenolic compounds are highly toxic compounds for health.
53 Nabi et al. [3] have studied the effect of these phenolic impurities on the combustion efficiency of the
54 biofuels. Their results have shown a decrease in the motor efficiency followed by the production of
55 toxic exhaust gases (NO and non-burned hydrocarbons) after the biofuels combustion step [3]. Such
56 reasons recommend the elimination of these phenol-type impurities to obtain ultra-pure bio-fuel. In

57 this work, we investigate a purification process based on the selective adsorption of phenolic
58 impurities in a semi-model biofuel mixture, using well-selected porous materials, with different
59 properties (porosity, acidity: type, amount and strength...), as adsorbents.

60 Adsorption is a well-known separation process [15]. It allows a selective capture of the undesired
61 product that can be further valorized, after a desorption step, for other applications. The adsorbents
62 must combine both high adsorption capacity and selectivity toward the molecules to eliminate [16]. In
63 addition, adsorbents regeneration under mild conditions is an important property that allows the reuse
64 of the adsorbents in several adsorption cycles [16–19]. Most of the studies dealing with the selective
65 adsorption of phenol and its derivatives were reported in aqueous solutions, in particular from
66 wastewater [16–18,20,21], since phenol and its derivatives are considered as priority pollutants even at
67 low concentration [22–26]. Roostaei et al. [27] studied the adsorption of phenol from water (2.2
68 mmol/L – 0.02 wt.%) using Y zeolites. During the adsorption, the equilibrium state was quickly
69 reached (0.27 mmol/g), and a reversible adsorption was obtained, after a regeneration step at 360°C
70 under air atmosphere for 16 hours [27]. For the same purpose, Khalid et al. [17] used Y zeolites, with
71 different Al loading ($5 < \text{Si}/\text{Al} < 100$), as adsorbents. They show that the high aluminum content in the
72 zeolite framework decreases the selectivity toward phenol molecules, due to the high affinity of
73 aluminum atoms for water molecules. At an initial phenol concentration of 17.4 mmol/L, the amount
74 of adsorbed phenol decreased from 50.5 mmol/g to 13 mmol/g when the Si/Al ratio decreases from
75 100 to 5, respectively [17]. The authors reported that, for an adsorption capacity of 50.5 mmol/g,
76 phenol molecules occupy only 20% of the micropore volume of the zeolite (0.285 cm³/g). The residual
77 pore volume in the zeolite was or inaccessible or filled by co-adsorbed water molecules that compete
78 phenol adsorption [17]. For both studies a comparison of the efficiency of zeolites adsorbents with
79 activated carbon, points out the highest adsorption capacity of this last adsorbent, especially for high
80 phenol concentration (> 13 mmol/L) [17,27]. However, its high regeneration cost, in comparison to
81 other adsorbents such as zeolites, limits its use for industrial realm [28–30].

82 On the other hand, only few studies dealt with the elimination of phenol derivates from hydrocarbons.
83 Two patents published in 1952 [31] and 1971 [32], studied respectively the phenol removing by
84 treating with a strong alkali metal hydroxide solution [31], and the phenol adsorption over
85 polyurethane foams followed by regeneration in acetone [32]. From that time, environmental standards
86 have widely changed, and these two processes remain far from the requirement of green chemistry. In
87 a previous work [33], we have studied the adsorption of phenol from isooctane and 1 wt.% n-nonane
88 using protonated HY zeolites with different Si/Al ratios (from 2.5 to 40). The composition of the
89 mixture was chosen in a way to allow studying the adsorption capacity of the zeolites towards phenol
90 in absence of any competition adsorbates. Phenol was adsorbed in both supercages and mesoporous
91 of the zeolites. Filling the supercage was conducted by the configuration of adsorbed phenol
92 molecules, whatever the Al loading, 3 phenol molecules were adsorbed in each supercage ($\approx 55\%$ of
93 the micropore volume). However, the parameters affecting the phenol adsorption in the mesoporous of
94 the zeolite were not investigated. Solids regeneration was shown to be limited by the number of the
95 total Brønsted (BAS) and Lewis (LAS) acid sites, and the quantification of the acid sites draws us to
96 conclude that one phenol molecule remains over each acid site [33]. In another work, DFT calculations
97 were used to calculate the interaction energies of phenol over BAS and LAS of HY zeolite (Si/Al =
98 47), and results confirm the low regeneration observed over high aluminum loaded zeolites ($E_{\text{phenol-BAS}}$
99 = -79 kJ/mol and $E_{\text{phenol-LAS}} = -199$ kJ/mol) [34]. Moreover, we showed the presence of two interaction
100 modes of phenol with the surface of the adsorbents: the first *via* its oxygen atom, while the second
101 corresponds to an interaction *via* its aromatic ring [34]. So far, the effect of the presence of aromatic
102 compounds, that corresponds to 30 – 50 vol.% of the 2nd generation biofuels fraction, was not studied
103 for phenol selective adsorption from biofuels. Regarding the used adsorbents, aromatic compounds
104 can widely affect the selectivity toward phenol adsorption, especially when weak interactions take
105 place or when phenol molecules are adsorbed *via* their aromatic ring. The aim of this paper is to study
106 the phenol selective adsorption for 2nd generation biofuels purification over low cost materials with
107 different textural properties and acidic strength. An understanding of the parameters that influence the
108 adsorption capacity of various adsorbent materials will be investigated. Moreover, the effect of the

109 strength of the OH groups on the selectivity toward phenol adsorption in presence of different
110 concentrations of aromatic compound (toluene) will be tackled to identify the parameters that can
111 inhibit the selective biofuels purification.

112 In this context, we propose adsorption process to study the selective removal of phenol from a
113 hydrocarbon mixture using a series of different solid adsorbents. Their performances are assessed in
114 term of the adsorption capacity, selectivity and ease of regeneration of the materials by measurements
115 with different mixtures containing phenol, n-nonane, isooctane and various amount of toluene (model
116 aromatic compound). Protonated Y zeolites with different Si/Al ratios (from 2.5 to 40) were firstly
117 selected to well understand the influence of the Si/Al ratio and the textural properties on the adsorption
118 capacity in batch and flow reactors. Secondly, the influence of the zeolitic structure was assessed by
119 comparing the performances of HY zeolites to that of ZSM-5 zeolite. Moreover, weak acid silica-
120 based solids (mesoporous and amorphous silica) and alumina were added to the series of tested
121 materials, and finally, the activities of all the adsorbents were compared to activated carbon, known as
122 a reference adsorbent.

123 **2. EXPERIMENTAL PART**

124 **2.1 Adsorbents**

125 NH_4^+Y zeolites with Si/Al ratio of 2.5 and 2.9 were supplied by Union Carbide. Ultra-stable HY
126 (USY) zeolites with various Si/Al ratios (22, 33, and 40) as well as proton exchanged ZSM-5 zeolite
127 (Si/Al = 42) were supplied by Zeolyst International. MCM-41 was prepared following the procedure
128 of Grün et al. [35]. Amorphous silica (Aerosil 200 from Degussa, called SiO_2 in the text), known as a
129 volatile material due to its very low density, was mixed with water (120% of its total pore volume) and
130 then calcined at 673 K to facilitate its use. The γ -alumina and the amorphous silica-alumina (called
131 ASA in the text - 99.1 wt.% SiO_2 , 0.9 wt.% Al_2O_3) solids were supplied respectively by Sasol and
132 Grace Davison. The activated carbon (called AC in the text), used as a reference adsorbent, was
133 provided by Norit.

134 2.2 Characterization techniques

135 The chemical composition of the zeolites was checked by inductively coupled plasma (ICP) optical
136 emission spectroscopy using a Varian ICP-OES 720-ES. Their textural properties were characterized
137 by nitrogen adsorption isotherms at 77K using gas adsorption system ASAP 2020 (Micrometrics) for a
138 relative pressure (P/P_0) varying between 0.05 and 1. Total and external surface areas were determined
139 using the Langmuir isotherms for the zeolites samples and α -plot method for the MCM-41 silica, with
140 LiChrospher Si-1000 Silica (surface area of 26.2 m²/g) as a reference [36]. Over the zeolite samples,
141 the external surface represents the surface of the outside of the zeolite grains as well as that of the
142 pores larger than micropores (>1.3 nm). For all the samples except zeolites, BET adsorption method
143 was applied to calculate the pore volume and the surface area.

144 The quantification of hydroxyl groups and acidic sites was performed using infrared (IR)
145 spectroscopy. Each sample was pressed, under a pressure of 10⁷ Pa, into a precisely weighted self-
146 supported wafer (10 - 15mg) with a surface of 2 cm². Prior to any experiment, sample wafer was pre-
147 treated *in-situ* in the IR cell by heating from 298K to 623K (1 K/min) followed by an isotherm at
148 623K for 4 hours under secondary vacuum (10⁻⁴ Pa). The FTIR spectrometer used was a Thermo
149 Fischer 6700 equipped with a MCT detector. 64 scans were accumulated for each measurement with a
150 resolution of 4 cm⁻¹. Note that the graphical resolution is greater than the spectral resolution and is
151 close to 0.5 cm⁻¹. The spectra displayed correspond to the difference between the spectrum after
152 adsorption (or desorption) and the spectrum corresponding to the activated (pre-treated) sample. All
153 spectra were normalized to a constant disc mass (5 mg/cm² of dried catalyst). To quantify the different
154 OH groups of the zeolites and the silica-based samples, four IR bands were taken into consideration :
155 (1) the $\nu(\text{OH})$ band at ~3645 cm⁻¹ that refers to zeolitic supercage OH groups of Y zeolites, that
156 presents a molar absorption coefficient of $\epsilon(\nu_{\text{OH supercage}}) = 7.5 \text{ cm}^2/\mu\text{mol}$, (2) the $\nu(\text{OH})$ band at ~3550
157 cm⁻¹ related to zeolitic sodalite cage OH groups of Y zeolites, the molar absorption coefficient of this
158 band is $\epsilon(\nu_{\text{OH sodalite cage}}) = 5.6 \text{ cm}^2/\mu\text{mol}$ [37], (3) the $\nu(\text{OH})$ band at ~3615 cm⁻¹ characteristic of the
159 framework OH groups of the ZSM-5 zeolite (molar absorption coefficient of $\epsilon(\nu_{\text{OH ZSM-5}}) = 3.5$

160 cm/ μmol [38], finally, (4) the combination band $(\nu+\delta)\text{OH}$ located at around 4600 cm^{-1} that refers to
161 silanol groups. Note that for silanol group, the quantification based on the area of the combination
162 band at 4600 cm^{-1} is preferred to that of the fundamental $\nu(\text{OH})$ at $\sim 3740\text{ cm}^{-1}$. Indeed, the molar
163 absorption coefficient of this latter, $\varepsilon(\nu_{\text{Si-OH}})$, strongly depends on H-bonding interactions [39], making
164 the area of the whole $\nu(\text{SiOH})$ massif not proportional to the Si-OH concentration. By contrast, it is
165 possible to accurately calculate the amount of silanol groups using the sharp $(\nu+\delta)\text{OH}$ combination
166 band located at about 4600 cm^{-1} with the molar extinction coefficient determined by Gallas *et al.*,
167 $\varepsilon_{(\nu+\delta)\text{OH}} = 0.16\text{ cm}/\mu\text{mol}$ [39].

168 For acid sites characterization, pyridine was used as probe molecule. After pretreating the solid wafer
169 in the IR cell, pyridine vapor was introduced at RT with calibrated doses from 0.05 to $1.70\ \mu\text{mol}$. A
170 final equilibrium pressure of 266 Pa was further established in the IR cell. Finally, thermal desorption
171 was carried out under secondary vacuum step by step from RT up to 423K for 20 minutes at each
172 temperature. Acidic sites of the solids were quantified from the IR spectra of the pyridine adsorbed
173 (Figure SI-1). The amount of Brønsted acid sites was determined by integrating the area of the
174 characteristic band ν_{8a} of the pyridinium ions (PyH^+) at 1545 cm^{-1} and using its corresponding molar
175 absorption coefficient: $\varepsilon(\text{PyH}^+) = 1.8\text{ cm}/\mu\text{mol}$ [37]. The amount of strong Lewis acid sites was
176 calculated using the molar absorption coefficient, $\varepsilon(\text{PyL}) = 1.5\text{ cm}/\mu\text{mol}$, of the band ν_{19b} at ~ 1445
177 cm^{-1} characteristic of the coordinated pyridine species (PyL) [37].

178 **2.3 Adsorption experiments**

179 Adsorption experiments were performed either in batch or in flow conditions. Phenol purchased from
180 Aldrich (99.5% purity) was used as a model molecule on all the adsorption studies. The liquid solution
181 containing phenol was obtained by dissolving 7.0 g (1 wt.%) of phenol into 1000 ml isooctane
182 (Aldrich 99+% purity). 1 wt.% of n-nonane (Aldrich 99.9% purity) was added as internal standard.
183 Further, the selective adsorption of phenol was studied by adding, to the previous mixture, various
184 concentrations of toluene (1, 10 and 40 wt.%) in a way to keep the same mass percent of phenol and n-
185 nonane (1 wt.%) in the whole mixture. For both batch and flow experiments, solids were pretreated *in-*

186 *situ* at 623K for 4 hours under argon flow before performing the adsorption experiments at room
187 temperature (25°C) and under atmospheric pressure. This activation allows the elimination of
188 physisorbed water as well as obtaining the acidic form of the zeolites i.e. H⁺Y from NH₄⁺Y zeolites.

189 For batch experiments, a specific system was developed allowing *in-situ* activation and transfer of the
190 powder into the hydrocarbon mixture under inert gas before the adsorption measurements (Figure SI-
191 2). In batch conditions, 0.3 g of solid, with a particle size ranging between 200 and 400 μm, were
192 poured into a two-neck round bottom flask (50 mL) containing 20 ml of the hydrocarbon mixture. The
193 flow adsorption tests were performed in a glass column (300 mm of high and 6 mm of internal
194 diameter). 0.5 g of adsorbent, with a particle size between 200 and 400 μm, were packed giving a bed
195 volume surging from 2 to 3 cm³. After the *in-situ* pretreatment stage, the solution to purify was fed
196 into the column using a Gilson pump allowing a constant flow rate of 1 ml/min. For batch and flow
197 systems, solution was collected periodically and analyzed using a Shimadzu 2010 gas chromatograph
198 equipped by a CP-sil 5CB capillary column (30 m), using a flame ionization detector and nitrogen as
199 carrier gas. Results of flow adsorption experiments were obtained as a breakthrough curve and the
200 amount of phenol adsorbed per gram of solid was calculated using the following formula (F₁):

201

$$(F_1) \quad q = \frac{C_0 \cdot D \cdot t_R}{m_{ads}}$$

202 where q is the amount of adsorbed phenol by gram of solid (mmol/g), C₀ is the initial phenol
203 concentration (mmol/L), D is the flow rate of the charge containing phenol (L/min), t_R corresponds to
204 the retention time (min) when the ratio of C_t/C₀ is equal to 0.5, and m_{ads} is the mass of the adsorbent
205 (g). The capacity of the most promising adsorbents to perform several runs was tested on additional
206 adsorption cycles performed after a thermal desorption at 473 K for 4 hours under Argon flow (90
207 ml/min).

208 3. RESULTS AND DISCUSSION

209 3.1 Adsorbents characterization

210 3.1.1 Textural properties

211 Table 1 gathers chemical and textural properties of the studied solids. N₂ adsorption isotherms are
212 presented in Figure SI-3. HY2.5 zeolite presents high surface area and high microporous volume. The
213 low external surface area and the negligible mesoporous volume is consistent with the quasi-absence
214 of defects in the zeolite structure. HY2.9 zeolite was obtained after dealuminating the parent HY2.5
215 zeolite without performing any acid washing, which explain its lower surface area, its slightly higher
216 external surface as well as the presence of some mesoporous volume in its structure, in comparison to
217 the parent HY2.5 zeolite. The greater Si/Al ratio of the USY zeolites (dealuminated zeolites) is
218 associated with the creation of mesopores (up to ~0.20 cm³/g) that increase the external surface area.
219 The ZSM-5 zeolite presents a total pore volume of 0.28 cm³/g, formed by both microporous (0.15
220 cm³/g) and mesoporous (0.13 cm³/g). The surface areas of the non-zeolitic metal oxides, i.e. SiO₂,
221 ASA, alumina and MCM-41, range from 203 to 984 m²/g. These non-zeolitic materials do not present
222 any micropores. By contrast, activated carbon presents a high surface area (1076 m²/g) and a pore
223 volume almost exclusively formed by micropores.

224 **Table 1 - Chemical and textural properties of the studied adsorbents.**

Adsorbents	Si/Al ^a at. ratio	Surface area (m ² /g)	External surface area (m ² /g) ^e	Pore volume (cm ³ /g) ^f		
				Total	Micro	Meso
HY2.5	2.5	1063 ^b	49 ^b	0.39	0.36	0.03
HY2.9	2.9	897 ^b	56 ^b	0.39	0.30	0.09
USY22	22	932 ^b	97 ^b	0.51	0.31	0.20
USY33	33	928 ^b	92 ^b	0.47	0.28	0.19
USY40	40	937 ^b	112 ^b	0.52	0.31	0.21
ZSM-5	42	458	150	0.28	0.15	0.13
SiO ₂	-	203 ^c	203	1.13	-	1.13
ASA	54	352 ^c	352	1.46	-	1.46
MCM-41	-	984 ^d	984	0.65 ^d	-	0.65 ^d

Al ₂ O ₃	-	326 ^c	326	0.78	-	0.78
AC	-	1076 ^c	34 ^e	0.61	0.54	0.07

225 ^a Measured by ICP ; ^b Determined using Langmuir isotherm ; ^c Determined using BET nitrogen
226 sorption ; ^d Determined using α -plot [36] ; ^e External surface = Surface of the outside of the zeolite
227 grains and of the pores larger than 1.3 nm ; ^f Determined using t-plot
228

229 3.1.2 Hydroxyl groups

230 Figure 1 displays the IR spectra in the $\nu(\text{OH})$ region of the most representative samples. HY2.5
231 features the well-known bands of bridged hydroxyls HF (high frequency) at 3645 cm⁻¹ (supercages
232 OH groups) and LF (low frequency) at 3550 cm⁻¹ (sodalite cages OH groups) of the Y zeolite, whereas
233 dealuminated HY2.9 zeolite shows the presence of three major additional OH bands at 3665, 3599 and
234 3535 cm⁻¹ characteristic of the presence of the amorphous phase. The band at 3599 cm⁻¹ is attributed in
235 the literature to superacid hydroxyl groups obtained from the interaction between the OH groups of the
236 supercage and the extraframework aluminum phase (EFAL) [37]. By analogy, the band at 3535 cm⁻¹
237 can be attributed to sodalite cages OH groups perturbed by the EFAL phase, and the band at 3665 cm⁻¹
238 is attributed to the OH groups of the EFAL phase. The steamed USY faujasites (only the spectra of
239 USY22 is shown) displayed an intense sharp band at almost 3740 cm⁻¹, assigned to external silanol
240 groups, in addition to low intense HF and LF $\nu(\text{OH})$ bands, which is in a good agreement with their
241 high Si/Al ratios. On ASA, SiO₂ and MCM-41, an intense and sharp SiOH band appears at 3747 cm⁻¹,
242 with a broad signal that extends down to 3400 cm⁻¹, associated to H-bonded SiOH groups. The spectra
243 of the ZSM-5 zeolite presents two bands: the first band at 3613 cm⁻¹ is characteristic vibration of the
244 framework OH groups whereas the second band at 3745 cm⁻¹ is attributed to the terminal silanol
245 groups of the external surface (Table 1) [40]. All these observations agree with the OH spectra
246 expected for the various adsorbents.

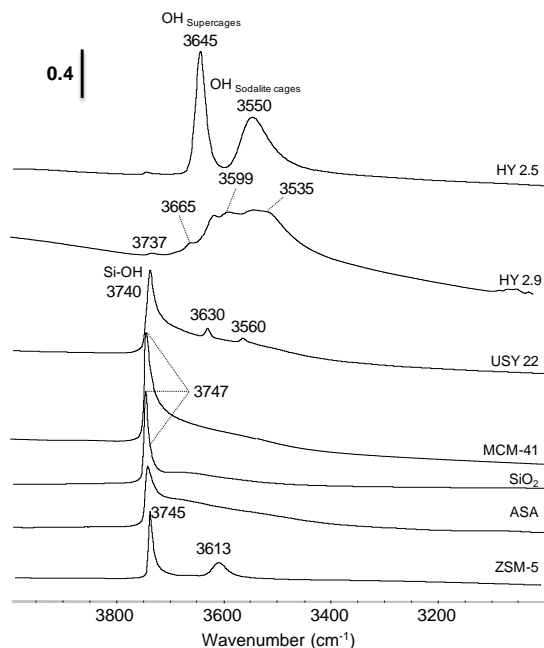


Figure 1 - Region of $\nu(\text{OH})$ bands ($3000 - 4000 \text{ cm}^{-1}$) of the different adsorbents after activation at 623 K under secondary vacuum.

247 The results of the quantification of the silanol groups, the HF and LF zeolitic OH groups of the various
 248 adsorbents are presented in Table 2. For silica-based samples, the amount of silanol groups increases
 249 with the surface area of these solids (Table 1). Over H-faujasites, the amount of silanol groups
 250 increases with the dealumination amount of the zeolitic framework (from 0 mmol of silanol per gram
 251 of HY2.5 zeolite up to 1.5 mmol of silanol per gram of USY40 zeolite). The formation of these silanol
 252 groups is related to the extraction of an aluminum atom from the zeolite structure that creates
 253 structural defects.

254 **Table 2 - Amount of silanol groups, zeolitic OH groups and acid sites over the various solids, as determined by IR**
 255 **spectroscopy.**

Adsorbent	Amount of OH groups ($\mu\text{mol/g}$)*			Amount of acid sites ($\mu\text{mol/g}$)*		
	SiOH	Supercage	Sodalite cage	BAS	LAS	Total
HY2.5	E	1160	2040	1263	22	1285
HY2.9	E	nd	nd	772	109	881
USY22	1210	45	58	136	189	325
USY33	1500	30	22	101	62	163
USY40	1550	22	25	60	17	77

ZSM-5	Nd	255 [#]	-	240	42	282
SiO ₂	1360	-	-	0	0	0
ASA	2320	-	-	14	71	85
MCM-41	3460	-	-	0	0	0

256 ϵ : Negligible; nd = not determined; # Framework OH groups; *: Data error analysis \pm 6 %.

257 3.1.3 Acid sites

258 The pyridine adsorption spectra, of the most representative samples, are shown in the Figure SI-1.
 259 HY2.5 presents almost exclusively BAS sites (bands at 1630-1620 and at 1545 cm⁻¹). The amount of
 260 BAS detected on this sample is consistent with the amount of supercage OH groups detected (Table 2
 261 – 1263 μ mol/g BAS in comparison to 1160 μ mol/g supercage OH groups). This points out that
 262 pyridinium ions cannot be formed over the sodalite OH groups of HY zeolite in particular for steric
 263 reasons [41]. Very few Lewis acid sites are detected on this sample in agreement with its absence of
 264 extraframework phase.

265 Over HY2.9 zeolite, pyridine adsorption confirms its dealumination by the detection of large amount
 266 of LAS (109 μ mol/g - Table 2). Pyridinium species are also present, however, the comparison with the
 267 amount of the OH groups in supercages and sodalite cages is not possible regarding the complexity of
 268 the IR spectrum (Figure 1).

269 For USY zeolites, the amount of pyridinium species formed is strongly smaller than for the parent
 270 HY2.5. This is consistent with the decrease of the amount of the zeolitic OH groups, due to
 271 dealumination. It should be noted that comparison between pyridinium species amount and
 272 concentration of OH groups reveals that the amount of BAS is greater to the total amount of supercage
 273 plus sodalite OH groups (USY22 - OH groups of supercage + sodalite cages = 103 μ mol/g; BAS =
 274 136 μ mol/g). Hence, contrary to HY, the strong acidic character of the zeolitic OH group of the
 275 dealuminated samples increases the mobility of the proton. This enables the protonation of pyridine
 276 molecules by the OH groups located in the sodalite cages [37]. The presence of acidic OH groups on
 277 the extraframework ASA phase of the USY zeolites should explained the greater amount of BAS
 278 detected compared to the amount of zeolitic OH groups [42]. The presence of some extraframework

279 phase is confirmed by the detection of strong LAS over USY. We can note that, as expected, the
280 strength of Brønsted acid sites increases with the dealumination of zeolite [43,44].

281 The ZSM-5 zeolite presents both Brønsted and Lewis acid sites, as evidenced by the bands
282 respectively at 1547 and 1456 cm^{-1} , giving a total number of 282 $\mu\text{mol/g}$ of acid sites. The amount of
283 Brønsted acid sites and that of zeolitic OH groups are in good agreement (240 $\mu\text{mol/g}$ OH per versus
284 282 $\mu\text{mol/g}$ acid sites). Over the SiO_2 and the MCM-41, no acid sites were detected which is in a good
285 agreement with the non-presence of aluminum atoms in these samples. In the case of ASA solid, low
286 amount of BAS and LAS was detected, as consequence with the high Si/Al ratio of this sample (Si/Al
287 = 54).

288 **3.2 Phenol adsorption capacities**

289 **3.2.1 Pretreatment effect on the phenol adsorption**

290 As shown in Table 2, all the studied zeolites present acid sites, that are known by their affinity toward
291 water adsorption [15,17]. Hence, the inhibitory effect of water on adsorbents over the phenol
292 adsorption was studied on zeolites and mesoporous MCM-41 silica in batch reactor.

293 In batch reactor, thermal treatments were performed in two different conditions. Firstly, *ex-situ*
294 pretreatment was performed to remove water from the adsorbents (623 K - 4h under Argon flow). The
295 pretreated solid was then quickly transferred under air atmosphere to the hydrocarbon solution. In a
296 second experiment, adsorbents were treated similarly using a home-built pretreatment cell (Figure SI-
297 2) that allows the transfer of the adsorbents, into the hydrocarbon solution, under inert atmosphere
298 (Argon), to avoid any water re-adsorption (*in-situ* pretreatment). Table 3 compares the amount of
299 adsorbed phenol measured for different adsorbents, after following different pre-treatments conditions.
300 Whatever *ex-situ* or *in-situ*, the pretreatment improves the adsorption capacity of all the studied
301 adsorbents except for MCM-41 (Table 3). The type of the pretreatment setup (*ex-situ* or *in-situ*) did
302 not lead to any beneficial effect over MCM-41 as well as over the zeolites with low aluminum loading.
303 Conversely, the *in-situ* pretreatment appears to be recommended to reach the maximum adsorption
304 capacity over high Al loaded zeolites. In the case of the *ex-situ* pretreatment, the short contact time of

305 these latter zeolites with the air moisture is enough to decrease their capacity toward phenol adsorption
 306 (Table 3). Figure 2 points out a direct correlation between the negative effect of the water contact on
 307 the amount of adsorbed phenol and the total amount of acidic sites (LAS + BAS - Table 2). Indeed, the
 308 phenol interaction energy with the protonic sites of H-faujasite (-85 kJ/mol), calculated using Grand
 309 Canonical Monte Carlo (GCMC) simulations, was found to be close to water interaction energy over
 310 the same site (-87.6 kJ/mol) [15]. Similar findings were observed by DFT calculations for the phenol
 311 and water interaction energies over extraframework LAS model (-199 kJ/mol for phenol in
 312 comparison to -190 kJ/mol for water) [34]. Thus, phenol molecules cannot displace all the water
 313 molecules, if these latter were already adsorbed on the acidic sites. We should mention that the
 314 absence of pretreatment effect for the MCM-41 agrees with the absence of any strong or medium
 315 acidic sites, as detected by pyridine adsorption (Table 2).

316 **Table 3 - Effect of the pretreatment conditions on the phenol adsorption capacity for the different adsorbents in batch**
 317 **reactor.**

Adsorbents	Amount of adsorbed phenol in batch reactor (mmol/g)		
	No pretreatment	<i>Ex-situ</i> retreatment	<i>In-situ</i> pretreatment
HY2.5	0.64	1.15	2.18
USY22	1.35	1.42	1.79
USY33	1.71	1.90	1.97
USY40	1.85	1.97	2.07
MCM-41	3.77	3.74	3.72

318
 319 Experiments performed under batch conditions points out that the pretreatment conditions (*in-situ*, *ex-*
 320 *situ*, no pretreatment) can strongly modify the adsorption capacity of the adsorbent. The more
 321 hydrophilic the zeolite is (low Si/Al ratio), the stronger is the inhibitory effect of water. This result is
 322 consistent with the numerous studies that points out the importance of hydrophobic character for
 323 phenol removal from wastewater [17,45]. Thus, as shown for HY2.5, even a very short contact with
 324 air atmosphere largely rehydrates the adsorbent and spoils its adsorption capacity (Table 3). Since the
 325 *in-situ* pretreatment can strongly improve the adsorption capacities (more than a factor 3 for HY2.5),
 326 in all the following experiments, solids were *in-situ* pre-treated prior adsorption tests.

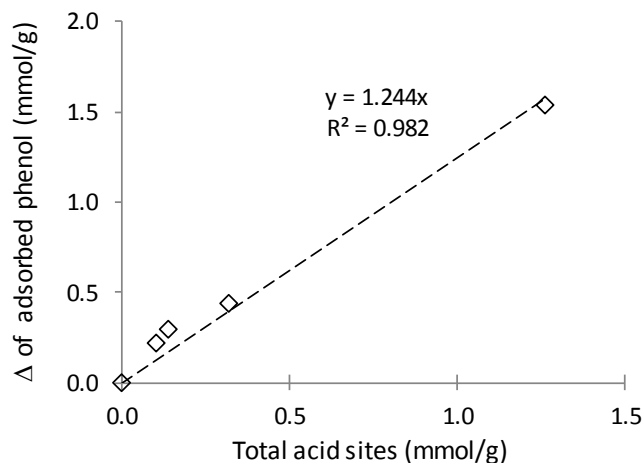
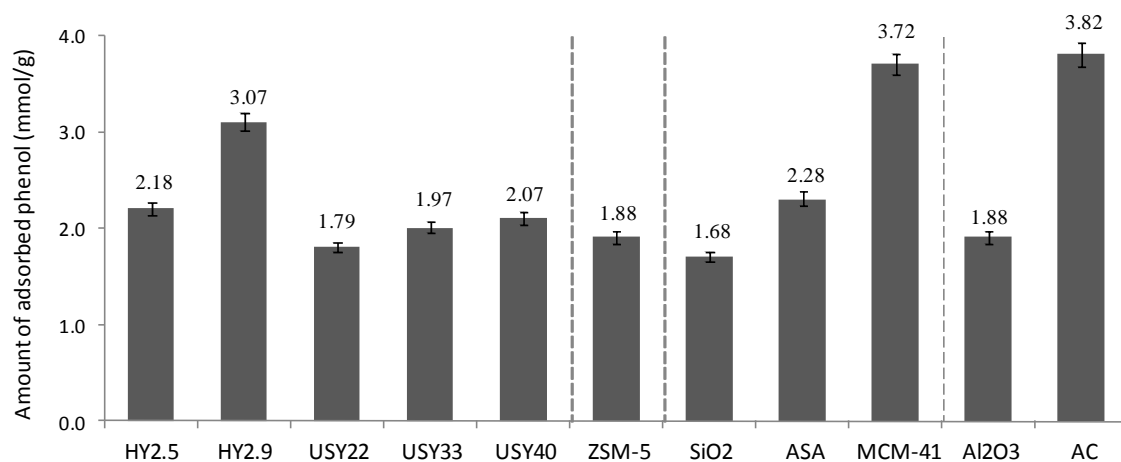


Figure 2 - Relation between the total amount of acid sites and the influence of the pretreatment over the different adsorbents. Δ = amount of adsorbed phenol with *in-situ* pretreatment at 623K minus amount of adsorbed phenol without pretreatment (batch reactor).

327 3.2.2 Phenol adsorption in the batch reactor

328 Figure 3 presents the adsorbed amounts of phenol by the different adsorbents, in batch reactor after *in-*
 329 *situ* activation at 623 K. Whatever the adsorbent, the adsorption phenomena is fast, and the
 330 equilibrium state is reached within few minutes. Figure 3 gives the percentage of phenol adsorbed
 331 after 1 hour over the various solids. In term of adsorption capacity, the most efficient adsorbents were
 332 mesoporous silica (MCM-41) and activated carbon, with almost 3.75 mmol of adsorbed phenol per
 333 gram of solid. For the silica-based solids (SiO_2 , ASA, MCM-41), the amount of adsorbed phenol is
 334 related to their surface area of these materials, as shown in Figure 4. The maximum adsorption
 335 capacity was obtained for MCM-41 that possesses the highest surface area in this series ($984 \text{ m}^2/\text{g}$).
 336 However, Y zeolites that also present high surface areas ($937 - 1015 \text{ m}^2/\text{g}$), have shown lower
 337 performances. Whatever their Si/Al ratio, all the H-faujasites present similar adsorption capacities
 338 (between 1.79 and 2.18 mmol/g), except for the HY2.9 zeolite that shows greater adsorption capacity
 339 (3.07 mmol/g). The high adsorption capacity of HY2.9 zeolite, in comparison to HY2.5 zeolite, can be
 340 caused by its relative higher accessibility obtained from the creation of mesoporous cavities (Table 1).
 341 The amount of adsorbed phenol over ZSM-5 zeolite (1.88 mmol/g) was similar to that obtained over
 342 the HY2.5 and USY zeolites. By contrast, ZSM-5 is the only adsorbent over which the n-nonane
 343 molecules were also adsorbed. This can be due to the small apertures of ZSM-5 pores ($5.5 \times 5.1 \text{ \AA}$)

344 that limit the accessibility of phenol molecules (kinetic diameter = 5.6 Å), in comparison to the big
 345 apertures of the Y zeolites supercages (7.4 x 7.4 Å) [46]. These small pores, non-filled with phenol,
 346 will be only accessible to the linear molecules, such as n-nonane. Hence, contrary to the Y zeolites, the
 347 ZSM-5 structure is not selective toward phenol adsorption in presence of linear hydrocarbons.
 348 Consequently, the ZSM-5 zeolite will not be studied in the flow adsorption section.



349

Figure 3 - Amount of adsorbed phenol from isooctane and 1 wt.% n-nonane mixture ($C_{\text{phenol}} = 74.4 \text{ mmol/L}$; $V = 20 \text{ mL}$) over the different solids after 1 h in batch reactor. The error bar values (3%) were calculated by carrying out 3 experiments under the same conditions.

350 Two main parameters should affect the phenol adsorption capacities of the adsorbents: (i) textural
 351 properties (the surface area, the porous volume and the pores size) and (ii) acidic properties (nature,
 352 strength, amount and accessibility of the acid sites).

353 *Effect of the textural properties*

354 As previously reported on a series of faujasite [33], the amount of phenol adsorbed on HY and USY
 355 strongly depends on the microporous volume of their supercages. Whatever the H-faujasite
 356 considered, a constant value of 3 phenol molecules per supercage was depicted through both
 357 experimental studies and theoretical calculations. On activated carbon that mainly presents
 358 micropores, the adsorption of phenol is due to capillary condensation inside the micropores.
 359 Nevertheless, phenol can be also adsorbed into the mesopores, as shown by the high adsorption
 360 capacities obtained on the solids that do not present any micropore system i.e. SiO₂, ASA and MCM-
 361 41 (Table 1 and Figure 3). Over these adsorbents, no correlation could be obtained between the

362 amounts of phenol and the mesoporous volume (not shown) whereas a good link with the surface area
 363 of the adsorbents was observed (Figure 4; circle). Hence the greater the specific surface of mesoporous
 364 solids, the greater the amount of phenol adsorbed.

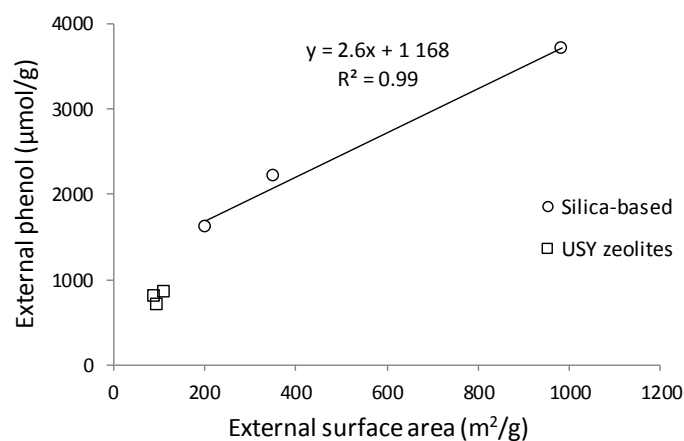


Figure 4 - Relationship between the amount of external phenol adsorbed (= total adsorbed phenol minus phenol adsorbed in micropores) and the external surface area of silica-based adsorbents and USY zeolites. Mixture of isooctane and 1wt.% n-nonane in batch reactor.

365 For USY zeolites that present both microporous and mesoporous systems, the amount of phenol
 366 specifically adsorbed into the micropores or into the mesopores can be assessed. Considering the total
 367 amount of adsorbed phenol and the fraction of microporous volume into the total porous volume
 368 ($V_{\text{micropores}}/V_{\text{total}}$), the quantity of “internal” phenol was calculated as reported in a previous work [33].
 369 Consequently, from the total amount of adsorbed phenol and from the amount of “internal” phenol, the
 370 amount of “external” phenol can be deduced (External phenol = Total phenol - internal phenol) (Table
 371 4). For all the USY samples, the amount of “external” phenol represents more than 60% of the total
 372 amount of phenol adsorbed. Table 4 pointed out that the ratios between the amount of “external”
 373 phenol and external surface stays close (~5 phenol molecules per nm²).

374 **Table 4 - Density of “external” phenol on the external surface of USY zeolites.**

Zeolites	Total phenol (μmol/g)	Internal phenol (μmol/g)	External phenol (μmol/g)	External surface (m ² /g)	External phenol (molecules/nm ²)
USY22	1790	1088	702	97	4.4
USY33	1970	1174	796	92	5.2
USY40	2070	1234	836	112	4.5

375 *Effect of the surface sites*

376 The nature and the amount of superficial sites can also influence the adsorption phenomena. Indeed, a
377 comparison of the amount of adsorbed phenol and the amount of silanol groups of silica-based
378 samples shows a linear regression, that goes through the origin point (Figure 5). Moreover, from the
379 value of the slope of the correlation (≈ 1), we can correspond one adsorbed phenol molecule to one
380 silanol group. Table 1 and Table 2 allow us to calculate the density of silanol per square nanometer. It
381 appears that the silanol density is lower on MCM-41 (2 SiOH/nm^2) than on silica and ASA (4
382 SiOH/nm^2) [47,48]. The variation of silanol group density among the silica-based sample explains
383 why the relationship presented Figure 4 does not go through the origin point. Hence, these
384 observations identify the increase in the density of silanol groups of silica-based samples as a key
385 parameter to improve their phenol adsorption capacity.

386 As for silanol groups of the USY zeolites, it has been previously reported that on dealuminated
387 zeolites, $\nu(\text{SiOH})$ band at 3740 cm^{-1} characterizes both external silanol (located in the mesopores and
388 on the outside surface of the zeolite grains) and internal silanol groups (defect sites of the supercage
389 and sodalite cages). These latter although not accessible, appears at the same frequencies than external
390 SiOH. Hence the amount of the silanol groups of USY reported on Figure 5 comprised both internal
391 and external SiOH groups. This explains why the total amount of silanol groups does not correlated
392 with the amount of external phenol. Thus, from this graph (see arrows of Figure 5), one can estimated
393 that the amount of silanol exceeding the linear correlation ($= \text{total silanol} - \text{external phenol}$) can be
394 attributed to internal silanol groups. This can be proposed as a method for determining the
395 accessibility of silanol groups of such zeolites.

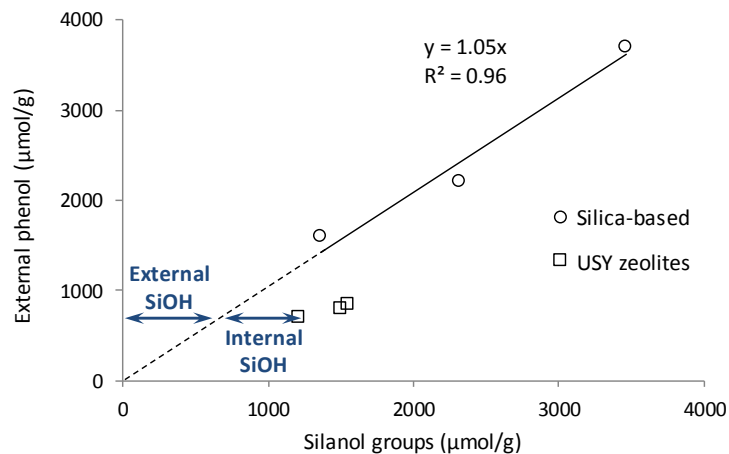


Figure 5 - Relationship between the amount of external phenol (= total adsorbed phenol minus internal phenol) and the amount of silanol groups of silica-based adsorbents and USY zeolites.

396 **3.2.3 Phenol adsorption in flow reactor**

397 The adsorption in a flow reactor is the most commonly adsorption method used in the industries. This
 398 method has the double advantages of making easier the *in-situ* activation of the adsorbent as well as its
 399 re-use for several adsorption runs after its *in-situ* regeneration between each two cycles. Only a
 400 selection of specific adsorbents was tested under flow conditions. In addition to MCM-41 (only silanol
 401 groups), alumina (strong acid sites) and activated carbon (reference adsorbent), a selection of Y
 402 zeolites was studied under these conditions. The zeolites were chosen in order to compare the effects
 403 of the Si/Al ratio and the acidity (and ratio) of the different OH groups (zeolitic OH groups and silanol
 404 groups).

405

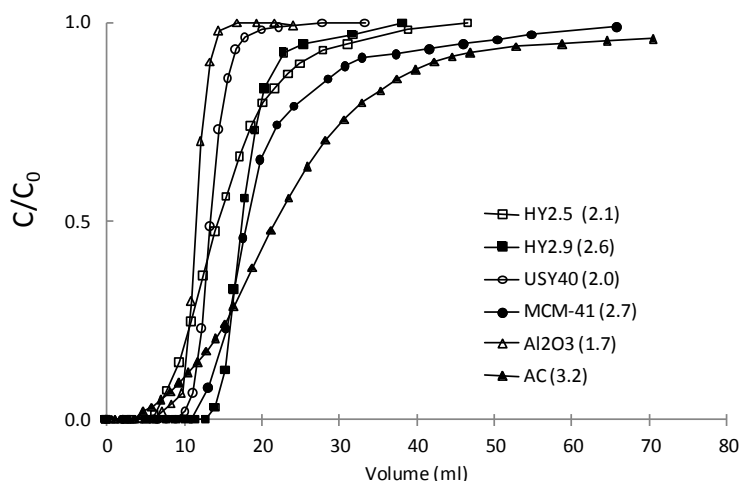


Figure 6 - Breakthrough curves of the phenol adsorption from isooctane mixture over the different adsorbents ($C_0 = 74.4$ mmol/L). Between the brackets is given the amount of adsorbed phenol over each adsorbent in mmol/g.

406 Figure 6 compared the breakthrough curves of the adsorbents for a phenol concentration of 74.4
 407 mmol/L in isooctane and 1 wt.% n-nonane. Using the formula (F1), from the section 2.3, and the
 408 specific retention time for each adsorbent, the amount of adsorbed phenol at saturation was calculated
 409 for each solid (Figure 7 - Cycle 1). Similar trends were observed in flow and batch conditions. The
 410 Si/Al ratio does not affect the adsorption capacity of HY2.5, and USY40 (~2 mmol/g) and HY2.9 still
 411 presents the greatest adsorption capacities (2.6 mmol/g) among the zeolite samples. A comparison of
 412 the mass-transfer zone or, equivalently, the difference between breakthrough and equilibration times,
 413 for HY2.5 and HY2.9 zeolites shows a shorter mass-transfer zone over the HY2.9 zeolite. The shorter
 414 the mass-transfer is, the most efficient is the adsorbent. The short mass-transfer zone of the HY2.9
 415 zeolite can be the reason of the higher accessibility, and thus the higher adsorption capacity, of HY2.9
 416 zeolite in comparison to HY2.5 zeolite. Al₂O₃ presents a lower adsorption capacity (1.7 mmol/g)
 417 compared to the other adsorbents, while MCM-41 and activated carbon maintained their high
 418 adsorption capacities with 2.7 and 3.2 mmol of adsorbed phenol per gram of solid, respectively.
 419 Hence, if the amount of adsorbed phenol was the only considered parameter, activated carbon would
 420 be considered as the best adsorbent. This result is not surprising since activated carbon is known for its
 421 high capacity of adsorption due to its high surface area and the capillary condensation occurring inside
 422 the pores [17,27,49]. However, another important parameter must be considered for larger scale

423 adsorption application: “*the breakthrough time (t_B)*”, that corresponds to the time during which the
 424 solids produce ultra-clean biofuel by adsorbing all the phenol molecules from the solution. Indeed,
 425 within the objective of developing an industrial process, the adsorption time during which ultra-pure
 426 biofuels are obtained (phenol molecules are completely removed) is the most important parameter.
 427 Figure 6 points out that the shape of the breakthrough curves can be very different as between the 3
 428 most performant adsorbents: HY2.9, MCM-41 and activated carbon. The activated carbon presents the
 429 shortest breakthrough time - $t_B = 4$ min. However, the phenol diffusion into the pores of activated
 430 carbon is slow and adsorption requires almost 50 minutes before reaching saturation. Otherwise, the
 431 breakthrough time is greater over MCM-41 - $t_B = 11$ min and similarly, due the low diffusion rate, the
 432 saturation takes almost 60 min to get reached. By contrast, HY2.9 zeolite was able to produce ultra-
 433 clean biofuel during 13 min, exceeding the breakthrough time of MCM-41 and activated carbon. A
 434 comparison between the adsorption capacities of HY2.9, MCM-41 and activated carbon using specific
 435 retention times and breakthrough times is shown in Table 5. By looking to the amount of phenol
 436 adsorbed at the breakthrough time, the zeolite HY2.9 shows the most promising results (1.9 mmol/g)
 437 in terms of providing the largest amount of ultrapure biofuel in one adsorption cycle, followed by the
 438 MCM-41 (1.3 mmol/g) and the USY40 zeolite (1.6 mmol/g), whereas the adsorption capacity of
 439 activated carbon drops to not more than 0.6 mmol/g, as shown in Table 5.

440 **Table 5 - Comparison between the amounts of phenol adsorbed using retention and breakthrough values for the most**
 441 **promising adsorbents.**

Adsorbents	Retention values		Breakthrough values	
	t_R (min)	Adsorbed phenol (mmol/g)	t_B (min)	Adsorbed phenol (mmol/g)
HY2.9	17.7	2.6	13	1.9
USY40	13.4	2.0	9	1.3
MCM-41	18.3	2.7	11	1.6
AC	21.3	3.2	4	0.6

442

443 3.3 Regeneration capacity of the adsorbents

444 The regeneration ability of the solids was studied on two adsorption-desorption cycles. To remove
445 phenol molecules adsorbed after cycle 1, a thermal desorption under Argon flow ($90\text{ cm}^3/\text{min}$) at 473
446 K for 4 hours was applied. After returning to 298 K, a second adsorption cycle was performed in the
447 same conditions as the first. Adsorption capacities of cycles 1 and 2 were compared in Figure 7.

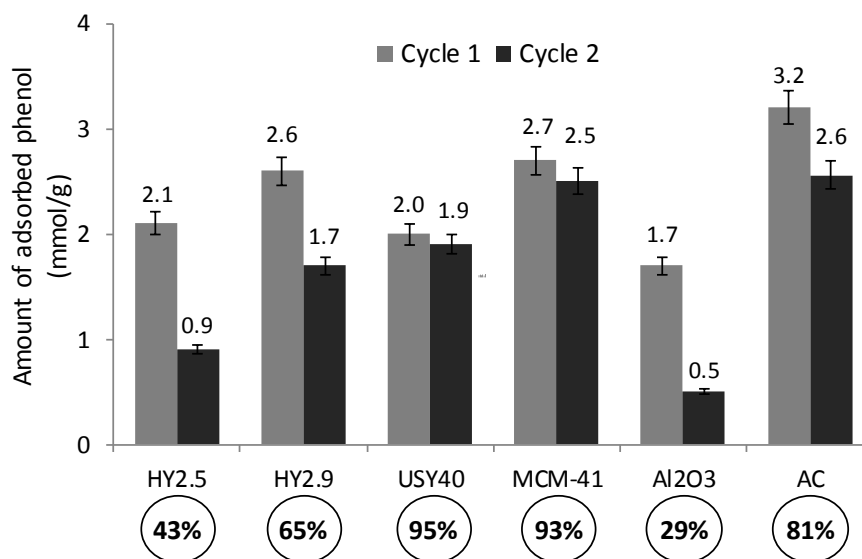


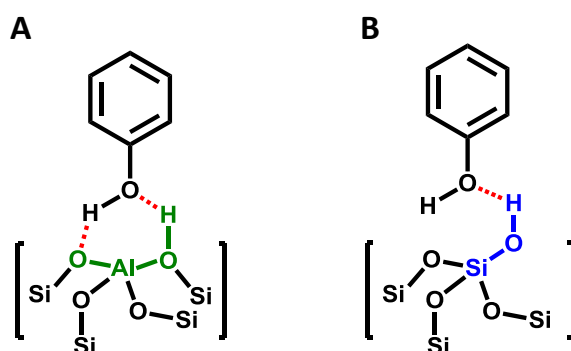
Figure 7 - Amount of adsorbed phenol over two consecutive adsorption cycles. Values in circles correspond to the regeneration percentages between the two adsorption cycles after a desorption step of 4 hours at 423K under Argon flow.

448 Figure 7 points out that Al_2O_3 presents the lowest regeneration capacity (29%). This is in line with
449 previous studies that showed that chemisorption of phenol over the strong Lewis acid sites of alumina
450 leads to the formation of phenolates species strongly held on surface [50]. By contrast, the activated
451 carbon presents a somewhat high regeneration capacity (81%) that is line with the phenol
452 condensation into AC micropores. After two adsorption cycles, AC presents equivalent adsorption
453 capacity than MCM-41. MCM-41 presents very high regeneration capacity equal to 93% over 2
454 adsorption cycles which is explained by the interaction of phenol molecules with the very weakly
455 acidic silanol groups located into the mesopores of MCM-41

456 Over the H-zeolites, the regeneration capacity increases with the Si/Al ratio (HY: 43%; HY2.9: 65%;
457 USY40: 95%). As shown in Figure SI-4, the amount of residual phenol (non-desorbed phenol species
458 by treatment at 473K) directly depends of the amount of acidic sites of the zeolites (BAS + LAS

459 quantified in Table 2) [33]. Hence, the presence of strongly acidic OH groups of the zeolites and
460 Lewis acid sites (Al^{3+}) limit the regeneration capacity of the different zeolites.

461 The results on the various zeolites also reveal that, for given conditions of regeneration, regenerability
462 changes with the amount of OH groups but not with their acidic strength. Once the strength is above a
463 certain value (in the present case: greater than that of silanol), the regeneration is limited.



465 **Figure 8 - Scheme for phenol adsorption on A) Acidic OH groups of zeolites; B) External silanol groups of silica-based**
466 **samples and USY zeolites.**

467 From the adsorption and regeneration properties, mechanisms for phenol adsorption on MCM and H-
468 faujasite can be proposed in Figure 8. For silica-based samples, the relationship between the amount of
469 phenol adsorbed and that of silanol groups (Fig. 5) indicates that one phenol is H-bonded to one
470 silanol groups, as depicted in Figure 8-B. The interaction with weakly acidic silanol groups is also
471 confirmed by the good regeneration capability of the MCM.

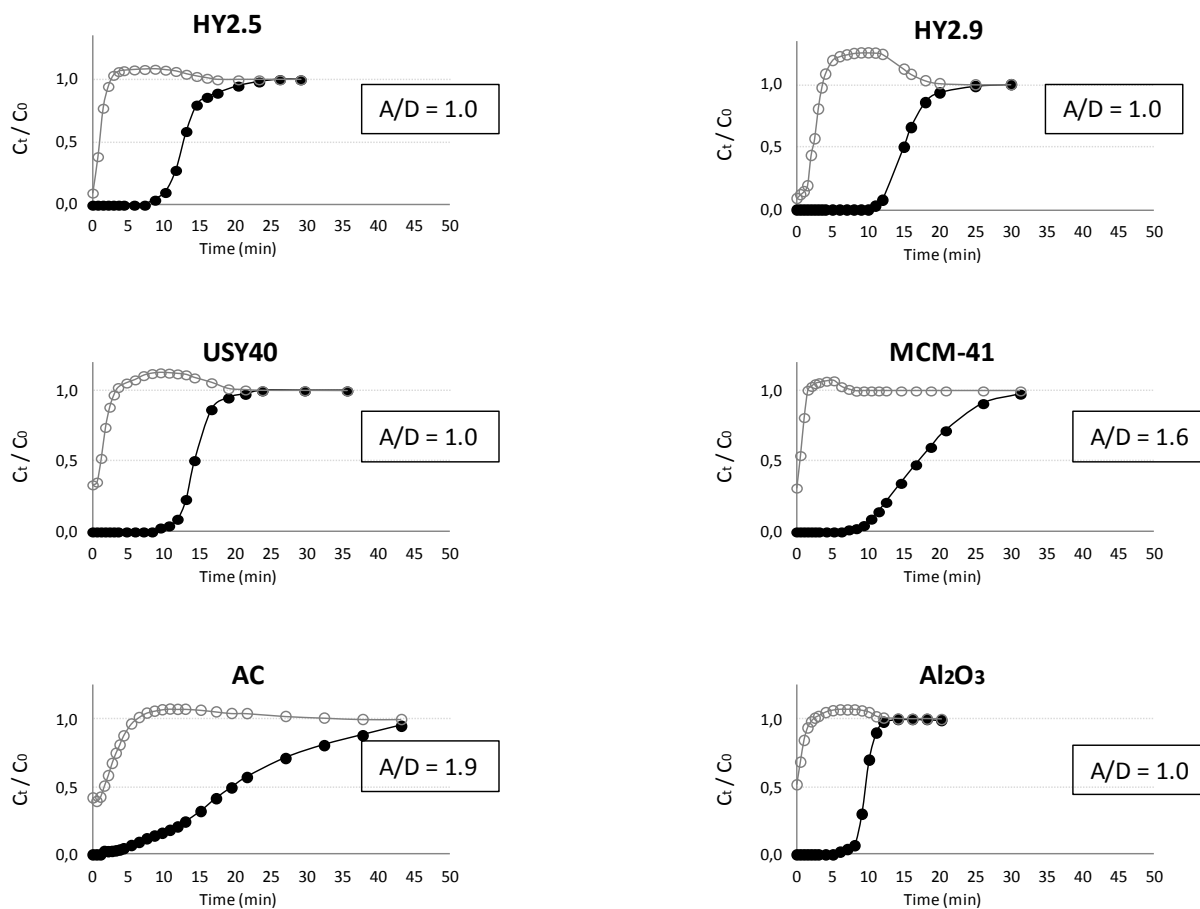
472 On the Y zeolites, the greater the amount of acidic sites, the lower the capability of regeneration
473 (Figure SI-4). This indicates that phenol interacts with zeolitic OH groups. This agrees with the DFT
474 computed model in a previous study [33], that shows that phenol interacts by its oxygen atom with the
475 proton zeolitic of the zeolite as depicted in Figure 8-A. The zeolitic OH group acidic strength being
476 greater than that of silanol groups, they retain more strongly the phenol, limiting the regeneration
477 capacity of Y zeolites with low Si/Al ratio.

478 These sections allow identifying the most promising adsorbents considering their adsorption and
479 regeneration capacities. The challenge that arises now concerns the selectivity of these adsorbents
480 toward phenol into a more complex hydrocarbon mixture containing an aromatic compound.

481 **3.4 Selective phenol adsorption in presence of toluene**

482 The selectivity toward phenol adsorption was tested under flow conditions from a mixture of 1 wt.%
483 phenol (74.4 mmol/L), 1 wt.% n-nonane and different concentrations of toluene (1 - 40 wt.%) into
484 isooctane. In a first step, the experiments were performed by flowing a solution of isooctane + 1 wt.%
485 n-nonane containing similar weight amount of phenol and toluene (1 wt.%) over a column filled with
486 0.5 g of the studied adsorbents. Six adsorbents were tested: HY2.5, HY2.9 and USY40 (to account for
487 the effect of the Si/Al ratio and absence/presence of EFAL phase), MCM-41 (to account for the
488 selectivity of the silanol groups), Al_2O_3 (to account for the selectivity of the aluminum coordinative
489 unsaturated sites) and activated carbon as a reference. The obtained breakthrough curves for phenol
490 and toluene are shown in Figure 9. Over all the series of adsorbents, initially phenol and toluene are
491 both adsorbed. However, toluene is eluted very rapidly and before the breakthrough of phenol. Phenol
492 adsorption is preferred over toluene for all adsorbents. It should be noted that at the beginning of the
493 toluene elution, a roll-up effect appears i.e. the concentration of toluene in the liquid phase is greater
494 than in the initial solution. This is explained by the fact that phenol molecules displace the already
495 adsorbed toluene molecules, and thus, the toluene concentration in the effluent surpass temporarily
496 that of the feed.

497



498

499 **Figure 9 - Breakthrough curves of phenol/toluene co-adsorption over various adsorbents. Full circle = Phenol; Open**
 500 **circle = toluene. A/D represents the ratio of the areas of adsorbed (A) and displaced (D) toluene (see Supplementary**
 501 **Information Figure SI-5).**

502 Even if all the solids show this roll-up effect for toluene indicating their preferential adsorption for
 503 phenol, its extent depends on the adsorbents. The ratio of the adsorbed toluene over the displaced
 504 toluene (A/D) was calculated for the various adsorbents by integrating the zones of adsorbed and
 505 displaced toluene as mentioned in Figure 9 (HY2.5).

506 Over activated carbon, the A/D value is 1.9 for a solution containing 1% toluene. This shows that
 507 activated carbon maintains some adsorbed toluene molecules in its cavities. Over activated carbon, the
 508 adsorption only occurs by capillary condensation inside the pores. Thus, there are no adsorption sites
 509 that can move the adsorption toward a specific molecule. For such a reason, the selectivity of activated
 510 carbon toward phenol is very weak in presence of toluene. As shown on Figure 9 and Table 6, the
 511 presence of toluene did not affect the adsorption capacity of Al₂O₃. Indeed, as mentioned before,
 512 phenol is so strongly adsorbed on alumina since the selectivity toward phenol reaches high values. On

513 protonated zeolite acid sites, HY2.5 (BAS), HY2.9 (BAS + LAS) as well as USY40 (lower amount of
514 BAS and LAS), phenol completely displaced all the adsorbed toluene molecules ($A/D \approx 1$). These
515 results can be explained by the respective strength of adsorption of phenol and toluene molecules with
516 the surface sites of the adsorbents. As shown previously by theoretical calculation on zeolites, the
517 toluene molecules can only be adsorbed by their aromatic cycle whereas phenol molecules can be
518 adsorbed both by their aromatic cycle or by their OH groups, even if this latter mode is favored [34].
519 Computed adsorption energy showed that, on zeolitic OH groups adsorption energy of phenol (-79
520 kJ/mol) is greater than that of toluene (-56 kJ/mol), confirming the preferential adsorption of phenol
521 on protonic zeolites. Over weak acid Si-OH groups (MCM-41 and main superficial sites over USY40)
522 the phenol is weakly adsorbed via its OH group; as confirmed by the high regeneration capacity of
523 these solids (Figure 7). However, this weak interaction was strong enough to maintain a selective
524 adsorption of phenol in presence of 1wt.% of toluene.

525 In a second step, the selectivity toward phenol adsorption was also tested with different mixtures
526 containing higher amount of toluene (10 and 40 wt.%, this latter corresponds to the amount of
527 aromatic compounds in second generation biofuels). The amount of adsorbed phenol was calculated,
528 as in the previous section (using the formula F1) and results are given in Table 6. As for activated
529 carbon, the increase of the concentration of toluene makes its poor selectivity more marked. Hence,
530 activated carbon is not satisfying adsorbent to purify a mixture of hydrocarbons. As for Al_2O_3 ,
531 whatever the toluene concentration, selectivity toward phenol remains intact. The less affected zeolites
532 by the increase of the amount of toluene are HY2.5 and HY2.9 zeolites, which reports the high
533 efficiency of strong acidic OH groups and LAS for the selective removal of phenol even in presence of
534 large amount of aromatic compounds. Regeneration experiments under the aforementioned conditions
535 (section 3.3) were also performed over HY2.5 and HY2.9 zeolites in presence of 40 wt.% toluene in
536 the mixture (Figure SI-6). Similar regeneration capacities as in the case of absence of toluene were
537 observed (45% and 63% for HY2.5 and HY2.9 zeolites, respectively).

538 **Table 6 - Amount of adsorbed phenol, measured in the flow reactor, in presence of different concentrations of toluene.**

Adsorbents	Amount of adsorbed phenol (mmol/g)			
	1% phenol 0% toluene	1% phenol 1% toluene	1% phenol 10% toluene	1% phenol 40% toluene
HY2.5	2.1	2.0	2.1	2.2
HY2.9	2.6	2.7	2.6	2.4
USY40	2.0	1.9	1.7	0.9
MCM-41	2.7	2.5	2.5	1.0
AC	3.2	2.7	1.7	0.4
Al ₂ O ₃	1.7	1.7	1.6	1.6

539

540 Over MCM-41 and USY40, the selectivity of weak acidic Si-OH groups was maintained until a
541 concentration of 10 wt.% of toluene in the solution. However, for 40 wt.% of toluene, the amount of
542 adsorbed phenol markedly decreases over these 2 solids (from 2.0 to 0.9 mmol/g over USY40 and
543 from 2.7 to 1.0 mmol/g over MCM-41). Since the adsorption being performed under dynamic
544 conditions, toluene molecules present in large quantity in the flow may train the weakly adsorbed
545 phenol molecules by π - π interaction (aromatic rings interaction). To verify this hypothesis, adsorption
546 experiments were performed after substituting the toluene by methylcyclohexane (MCH) in order to
547 remove the effect of the π - π interactions. Results, presented in Table 7, prove that the adsorption
548 capacities for phenol of the MCM-41 and USY40 are not affected by the presence of
549 methylcyclohexane. This confirms that a solvation effect occurs with π - π interaction of the molecules
550 in the flow prevents the trapping of phenol on the weak adsorption sites (Si-OH groups) of the
551 adsorbents.

552 **Table 7 – Amount of adsorbed phenol over MCM-41 and USY40 in presence of 40 wt.% of toluene or MCH.**

Adsorbents	Amount of adsorbed phenol (mmol/g)		
	1% phenol 0% toluene	1% phenol 40% toluene	1% phenol 40% MCH
USY40	2.0	0.9	1.9
MCM-41	2.7	1.0	2.8

553

554 CONCLUSION

555 The present study deals with the selective removal of phenol from a semi-model biofuel mixture.
556 Various types of adsorbents i.e. Y, USY and ZSM-5 zeolites, silica-based oxides, aluminum oxide and
557 activated carbon, that present different structural, textural and acidic properties were tested.

558 - Micropores and mesopores of the Y zeolites are both involved in the phenol adsorption although in a
559 very different way. Phenol is condensed into the micropores of the Y zeolites and an amount of 3
560 phenol molecules per supercage was measured on the different faujasites. Such fraction of phenol
561 called “internal phenol” is directly related to the porous volume of the crystalline fraction of the
562 zeolite. In the same manner, AC with its great microporous network also presents high phenol
563 adsorption capacities. Note that, in the zeolitic micropores with entrance lower than 6 Å, as for Y
564 sodalite cage and ZSM-5 pores, the phenol adsorption is very limited. Additional amount of phenol,
565 called “external phenol” are adsorbed on the silanol groups of the mesoporous cavities of the zeolites
566 (created by dealumination). On silica-based solids that present only mesopores, the present study
567 establishes that one phenol molecule interacts with one silanol group. Thus, the phenol adsorption
568 capacity in the mesopores is directly correlated to the concentration of silanol groups.

569 - Acidic properties of the adsorbents strongly impact their selectivity. In presence of 1 - 10 wt.%
570 toluene, HY and USY zeolites and MCM-41 present good phenol adsorption capacities. By contrast, a
571 greater amount of toluene (40 wt.%) strongly decreases the selectivity for phenol adsorption over USY
572 and MCM-41. This is explained by the solvation effect that affect the weak acidic silanol groups,
573 largely present over these solids, and thus prohibits them from adsorbing phenol under such condition.
574 Although activated carbon that presents high phenol adsorption capacities in simple mixture, has
575 shown a very poor selectivity toward phenol in more complex hydrocarbon mixtures, due to the
576 absence of acidic properties. Hence to selectively adsorb phenol, large amount of strongly acidic
577 sites is required as over HY2.5 and HY2.9 zeolites.

578 - Acidic properties were shown to negatively influence the regenerability of the adsorbents. To
579 regenerate the adsorbents under mild conditions, the amount of strong Brønsted or Lewis acidic sites

580 must be limited since they strongly retain phenol. Thus, the best regeneration capacities are obtained
581 on USY and MCM-41.

582 Hence, this study allows rationalizing the impact of the micro- and mesoporous texture as well as the
583 location, nature and strength of the acidic sites on their adsorption capacities, selectivity and
584 regeneration abilities. The best compromise between adsorption capacity, selectivity toward phenol
585 and regeneration ability was obtained with HY2.9 zeolite, i.e. the solid that presents large amount of
586 micropores, some mesopores and an intermediate amount of strongly acidic sites. This allows
587 obtaining good adsorption capacity, maintaining a high selectivity and acceptable regeneration.

588 **ACKNOWLEDGMENTS**

589 We thank the Labex EMC3, ANR and FEDER for the PhD grant of IK and for the financial support to
590 the BIOCAR project. We also thank Benjamin FOUCAULT and Adrien LANEL for helping in
591 installation, design and realization of adsorption setup.

592 **REFERENCES**

- 593 [1] BP Energy Outlook 2018, (2018) 125.
- 594 [2] M. Bertero, G. de la Puente, U. Sedran, Fuels from bio-oils: Bio-oil production from
595 different residual sources, characterization and thermal conditioning, *Fuel*. 95 (2012)
596 263–271. doi:10.1016/j.fuel.2011.08.041.
- 597 [3] M.N. Nabi, M.M. Rahman, M.A. Islam, F.M. Hossain, P. Brooks, W.N. Rowlands, J.
598 Tulloch, Z.D. Ristovski, R.J. Brown, Fuel characterisation, engine performance,
599 combustion and exhaust emissions with a new renewable Licella biofuel, *Energy*
600 *Conversion and Management*. 96 (2015) 588–598. doi:10.1016/j.enconman.2015.02.085.
- 601 [4] G. Fogassy, N. Thegarid, Y. Schuurman, C. Mirodatos, From biomass to bio-gasoline by
602 FCC co-processing: effect of feed composition and catalyst structure on product quality,
603 *Energy & Environmental Science*. 4 (2011) 5068. doi:10.1039/c1ee02012a.
- 604 [5] S.S. Reham, H.H. Masjuki, M.A. Kalam, I. Shancita, I.M. Rizwanul Fattah, A.M. Ruhul,
605 Study on stability, fuel properties, engine combustion, performance and emission
606 characteristics of biofuel emulsion, *Renewable and Sustainable Energy Reviews*. 52
607 (2015) 1566–1579. doi:10.1016/j.rser.2015.08.013.
- 608 [6] J.C. Serrano-Ruiz, J.A. Dumesic, Catalytic routes for the conversion of biomass into
609 liquid hydrocarbon transportation fuels, *Energy and Environmental Science*. 4 (2011)
610 83–99. doi:10.1039/C0EE00436G.
- 611 [7] G. Fogassy, C. Lorentz, G. Toussaint, N. Thegarid, Y. Schuurman, C. Mirodatos,
612 Analytical techniques tailored for biomass transformation to biofuels, *Environmental*
613 *Progress & Sustainable Energy*. 32 (2013) 377–383. doi:10.1002/ep.10631.
- 614 [8] F. de Miguel Mercader, M.J. Groeneveld, S.R.A. Kersten, N.W.J. Way, C.J. Schaverien,
615 J.A. Hogendoorn, Production of advanced biofuels: Co-processing of upgraded pyrolysis
616 oil in standard refinery units, *Applied Catalysis B: Environmental*. 96 (2010) 57–66.
617 doi:10.1016/j.apcatb.2010.01.033.
- 618 [9] E.-M. Aro, From first generation biofuels to advanced solar biofuels, *Ambio*. 45 (2016)
619 24–31. doi:10.1007/s13280-015-0730-0.
- 620 [10] R. Chaudhary, P.L. Dhepe, Solid base catalyzed depolymerization of lignin into low
621 molecular weight products, *Green Chemistry*. 19 (2017) 778–788.
622 doi:10.1039/C6GC02701F.
- 623 [11] C. Bouvier, Y. Romero, F. Richard, S. Brunet, Effect of H₂S and CO on the
624 transformation of 2-ethylphenol as a model compound of bio-crude over sulfided Mo-
625 based catalysts: propositions of promoted active sites for deoxygenation pathways based
626 on an experimental study, *Green Chemistry*. 13 (2011) 2441. doi:10.1039/c1gc15181a.
- 627 [12] G.W. Huber, S. Iborra, A. Corma, Synthesis of Transportation Fuels from Biomass:
628 Chemistry, Catalysts, and Engineering, *Chemical Reviews*. 106 (2006) 4044–4098.
629 doi:10.1021/cr068360d.
- 630 [13] Z. Zhang, Q. Wang, P. Tripathi, C.U. Pittman Jr, Catalytic upgrading of bio-oil using 1-
631 octene and 1-butanol over sulfonic acid resin catalysts, *Green Chemistry*. 13 (2011) 940.
632 doi:10.1039/c0gc00464b.
- 633 [14] M. Bertero, U. Sedran, Upgrading of bio-oils over equilibrium FCC catalysts.
634 Contribution from alcohols, phenols and aromatic ethers, *Catalysis Today*. 212 (2013)
635 10–15. doi:10.1016/j.cattod.2013.03.016.
- 636 [15] F. Ektefa, S. Javadian, M. Rahmati, Computational comparison of the efficiency of
637 nanoporous zeolite frameworks for separation of phenol from water, *Journal of the*
638 *Taiwan Institute of Chemical Engineers*. 88 (2018) 104–113.
639 doi:10.1016/j.jtice.2018.03.020.

- 640 [16] B. Koubaissy, G. Joly, I. Batonneau-Gener, P. Magnoux, Adsorptive Removal of
641 Aromatic Compounds Present in Wastewater by Using Dealuminated Faujasite Zeolite,
642 Industrial & Engineering Chemistry Research. 50 (2011) 5705–5713.
643 doi:10.1021/ie100420q.
- 644 [17] M. Khalid, G. Joly, A. Renaud, P. Magnoux, Removal of Phenol from Water by
645 Adsorption Using Zeolites, Industrial & Engineering Chemistry Research. 43 (2004)
646 5275–5280. doi:10.1021/ie0400447.
- 647 [18] B. Van de Voorde, D. Damasceno Borges, F. Vermoortele, R. Wouters, B. Bozbiyik, J.
648 Denayer, F. Taulelle, C. Martineau, C. Serre, G. Maurin, D. De Vos, Isolation of
649 Renewable Phenolics by Adsorption on Ultrastable Hydrophobic MIL-140 Metal–
650 Organic Frameworks, ChemSusChem. 8 (2015) 3159–3166.
651 doi:10.1002/cssc.201500281.
- 652 [19] L. Damjanović, V. Rakić, V. Rac, D. Stošić, A. Auroux, The investigation of phenol
653 removal from aqueous solutions by zeolites as solid adsorbents, Journal of Hazardous
654 Materials. 184 (2010) 477–484. doi:10.1016/j.jhazmat.2010.08.059.
- 655 [20] W. Kujawski, A. Warszawski, W. Ratajczak, T. Porebski, W. Capa\la, I. Ostrowska,
656 Removal of phenol from wastewater by different separation techniques, Desalination.
657 163 (2004) 287–296.
- 658 [21] S. Petkovic, B. Adnadjevic, J. Jovanovic, Novel kinetics model for adsorption of
659 pollutant from wastewaters onto zeolites. Kinetics of phenol adsorption on zeolite-type
660 silicalite, Adsorption Science & Technology. 37 (2019) 349–364.
661 doi:10.1177/0263617419833201.
- 662 [22] O. Hamdaoui, E. Naffrechoux, Modeling of adsorption isotherms of phenol and
663 chlorophenols onto granular activated carbon Part II. Models with more than two
664 parameters, Journal of Hazardous Materials. 147 (2007) 401–411.
665 doi:10.1016/j.jhazmat.2007.01.023.
- 666 [23] G.D. Sheng, D.D. Shao, X.M. Ren, X.Q. Wang, J.X. Li, Y.X. Chen, X.K. Wang,
667 Kinetics and thermodynamics of adsorption of ionizable aromatic compounds from
668 aqueous solutions by as-prepared and oxidized multiwalled carbon nanotubes, Journal of
669 Hazardous Materials. 178 (2010) 505–516. doi:10.1016/j.jhazmat.2010.01.110.
- 670 [24] N.A. Khan, Z. Hasan, S.H. Jhung, Adsorptive removal of hazardous materials using
671 metal-organic frameworks (MOFs): A review, Journal of Hazardous Materials. 244–245
672 (2013) 444–456. doi:10.1016/j.jhazmat.2012.11.011.
- 673 [25] B.H. Hameed, A.A. Rahman, Removal of phenol from aqueous solutions by adsorption
674 onto activated carbon prepared from biomass material, Journal of Hazardous Materials.
675 160 (2008) 576–581. doi:10.1016/j.jhazmat.2008.03.028.
- 676 [26] T. Viraraghavan, F. de Maria Alfaro, Adsorption of phenol from wastewater by peat, fly
677 ash and bentonite, Journal of Hazardous Materials. 57 (1998) 59–70.
678 doi:10.1016/S0304-3894(97)00062-9.
- 679 [27] N. Roostaei, F.H. Tezel, Removal of phenol from aqueous solutions by adsorption,
680 Journal of Environmental Management. 70 (2004) 157–164.
681 doi:10.1016/j.jenvman.2003.11.004.
- 682 [28] D. Hank, Z. Azi, S. Ait Hocine, O. Chaalal, A. Hellal, Optimization of phenol adsorption
683 onto bentonite by factorial design methodology, Journal of Industrial and Engineering
684 Chemistry. 20 (2014) 2256–2263. doi:10.1016/j.jiec.2013.09.058.
- 685 [29] S. Babel, Low-cost adsorbents for heavy metals uptake from contaminated water: a
686 review, Journal of Hazardous Materials. 97 (2003) 219–243. doi:10.1016/S0304-
687 3894(02)00263-7.

- 688 [30] T. Mathialagan, T. Viraraghavan, Adsorption of cadmium from aqueous solutions by
689 perlite, *Journal of Hazardous Materials*. 94 (2002) 291–303. doi:10.1016/S0304-
690 3894(02)00084-5.
- 691 [31] F.P. Lobban, Process for removing phenols and mercaptans from light petroleum
692 distillates, US patent 2605212, 1952.
- 693 [32] R.C. Schlicht, F.C. McCoy, Selective adsorption of phenols from solution in
694 hydrocarbons, US Patent 3617531, 1971.
- 695 [33] I. Khalil, H. Jabraoui, G. Maurin, S. Lebègue, M. Badawi, K. Thomas, F. Maugé,
696 Selective Capture of Phenol from Biofuel Using Protonated Faujasite Zeolites with
697 Different Si/Al Ratios, *The Journal of Physical Chemistry C*. 122 (2018) 26419–26429.
698 doi:10.1021/acs.jpcc.8b07875.
- 699 [34] H. Jabraoui, I. Khalil, S. Lébegue, M. Badawi, Ab Initio Screening of Cation-Exchanged
700 Zeolites for Biofuel Purification, *Molecular Systems Design & Engineering*. (2019)
701 10.1039/C9ME00015A. doi:10.1039/C9ME00015A.
- 702 [35] M. Grün, K.K. Unger, A. Matsumoto, K. Tsutsumi, Novel pathways for the preparation
703 of mesoporous MCM-41 materials: control of porosity and morphology, *Microporous
704 and Mesoporous Materials*. 27 (1999) 207–216. doi:10.1016/S1387-1811(98)00255-8.
- 705 [36] M. Kruk, M. Jaroniec, C.H. Ko, R. Ryoo, Characterization of the Porous Structure of
706 SBA-15, *Chemistry of Materials*. 12 (2000) 1961–1968. doi:10.1021/cm000164e.
- 707 [37] S. Khabtou, T. Chevreau, J.C. Lavalley, Quantitative infrared study of the distinct acidic
708 hydroxyl groups contained in modified Y zeolites, *Microporous Materials*. 3 (1994)
709 133–148. doi:10.1016/0927-6513(94)00015-8.
- 710 [38] H. Li, S.A. Kadam, A. Vimont, R.F. Wormsbecher, A. Travert, Monomolecular
711 Cracking Rates of Light Alkanes over Zeolites Determined by IR Operando
712 Spectroscopy, *ACS Catalysis*. 6 (2016) 4536–4548. doi:10.1021/acscatal.6b01025.
- 713 [39] J.-P. Gallas, J.-M. Goupil, A. Vimont, J.-C. Lavalley, B. Gil, J.-P. Gilson, O. Miserque,
714 Quantification of Water and Silanol Species on Various Silicas by Coupling IR
715 Spectroscopy and in-Situ Thermogravimetry, *Langmuir Article*. 25 (2009) 5825–5834.
- 716 [40] P.A. Jacobs, R. Von Ballmoos, Framework hydroxyl groups of H-ZSM-5 zeolites, *The
717 Journal of Physical Chemistry*. 86 (1982) 3050–3052. doi:10.1021/j100212a046.
- 718 [41] F. Thibault-Starzyk, B. Gil, S. Aiello, T. Chevreau, J.-P. Gilson, In situ
719 thermogravimetry in an infrared spectrometer: an answer to quantitative spectroscopy of
720 adsorbed species on heterogeneous catalysts, *Microporous and Mesoporous Materials*.
721 67 (2004) 107–112. doi:10.1016/j.micromeso.2003.10.016.
- 722 [42] O. Cairon, T. Chevreau, J.-C. Lavalley, Brønsted acidity of extraframework debris in
723 steamed Y zeolites from the FTIR study of CO adsorption, *Journal of the Chemical
724 Society, Faraday Transactions*. 94 (1998) 3039–3047.
- 725 [43] K. Thomas, C. Binet, T. Chevreau, D. Cornet, J.-P. Gilson, Hydrogenation of Toluene
726 over Supported Pt and Pd Catalysts: Influence of Structural Factors on the Sulfur
727 Tolerance, *Journal of Catalysis*. 212 (2002) 63–75. doi:10.1006/jcat.2002.3780.
- 728 [44] G. Crépeau, V. Montouillout, A. Vimont, L. Mariey, T. Cseri, F. Maugé, Nature,
729 Structure and Strength of the Acidic Sites of Amorphous Silica Alumina: An IR and
730 NMR Study, *The Journal of Physical Chemistry B*. 110 (2006) 15172–15185.
731 doi:10.1021/jp062252d.
- 732 [45] P. Kowalczyk, A. Deditius, W.P. Ela, M. Wiśniewski, P.A. Gauden, A.P. Terzyk, S.
733 Furmaniak, J. Włoch, K. Kaneko, A.V. Neimark, Super-sieving effect in phenol
734 adsorption from aqueous solutions on nanoporous carbon beads, *Carbon*. 135 (2018) 12–
735 20. doi:10.1016/j.carbon.2018.03.063.

- 736 [46] C. Baerlocher, L.B. McCusker, D.H. Olson, Atlas of zeolite framework types, 6th rev.
737 ed, Elsevier, page 141, Amsterdam, 2007.
- 738 [47] T. Martin, B. Lefevre, D. Brunel, A. Galarneau, F. Di Renzo, F. Fajula, P.F. Gobin, J.F.
739 Quinson, G. Vigier, Dissipative water intrusion in hydrophobic MCM-41 type materials,
740 Chemical Communications. 1 (2002) 24–25. doi:10.1039/b109081j.
- 741 [48] A. Cauvel, D. Brunel, F. Di Renzo, E. Garrone, B. Fubini, Hydrophobic and Hydrophilic
742 Behavior of Micelle-Templated Mesoporous Silica, Langmuir. 13 (1997) 2773–2778.
743 doi:10.1021/la962059i.
- 744 [49] A.T. Mohd Din, B.H. Hameed, A.L. Ahmad, Batch adsorption of phenol onto
745 physiochemical-activated coconut shell, Journal of Hazardous Materials. 161 (2009)
746 1522–1529. doi:10.1016/j.jhazmat.2008.05.009.
- 747 [50] A. Popov, E. Kondratieva, L. Mariey, J.M. Goupil, J. El Fallah, J.-P. Gilson, A. Travert,
748 F. Maugé, Bio-oil hydrodeoxygenation: Adsorption of phenolic compounds on sulfided
749 (Co)Mo catalysts, Journal of Catalysis. 297 (2013) 176–186.
750 doi:10.1016/j.jcat.2012.10.005.
751